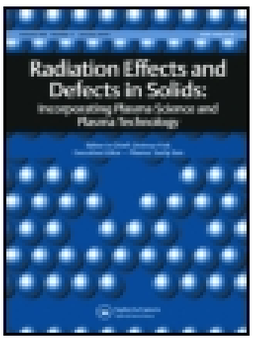

Taylor & Francis
Taylor & Francis Group

Radiation Effects and Defects in Solids
Incorporating Plasma Science and Plasma Technology

ISSN: (Print) (Online) Journal homepage: https://www.tandfonline.com/loi/grad20

Analysis of neutron emission in a dense plasma focus device

A. Raeisdana , S. M. Sadat Kiai , A. Sadighzadeh , A. Ghorbani & M. Bakhshzad Mahmoudi

To cite this article: A. Raeisdana , S. M. Sadat Kiai , A. Sadighzadeh , A. Ghorbani & M. Bakhshzad Mahmoudi (2020): Analysis of neutron emission in a dense plasma focus device, Radiation Effects and Defects in Solids, DOI: 10.1080/10420150.2020.1821683

To link to this article: https://doi.org/10.1080/10420150.2020.1821683

RADIATION EFFECTS & DEFECTS IN SOLIDS
https://doi.org/10.1080/10420150.2020.1821683

Taylor & Francis
Taylor & Francis Group

Analysis of neutron emission in a dense plasma focus device

A. Raeisdana, S. M. Sadat Kiai, A. Sadighzadeh, A. Ghorbani and M. Bakhshzad Mahmoudi

Plasma and Nuclear Fusion Research School, Nuclear Science & Technology Research Institute, Atomic Energy Organization of Iran, Tehran, Iran

ABSTRACT

Time of flight method is used to determine the emitted pulsed neutron energy spectrum from the $D(D,n)^3He$ and $D(T,n)^4He$ reactions in the IR-MPF-100 (115 kJ, 40 kV, 144 μF), dense plasma focus device (DPF). D-D and D-T neutrons were detected by NE-102 plastic scintillator photomultiplier (PS-PM) detector. The PS-PM detector has been located 2.5 m away from the focus region at the angle of 90° with respect to the device axis. Results display 1.51–2.75 MeV and 1.79–2.97 MeV energies for D-D neutrons and 12.09 ± 0.4 MeV energy for D-T neutrons. Fusion chained reactions have been studied. Scattered neutrons are detected and their energies are computed.

ARTICLE HISTORY
Received 5 September 2020
Accepted 7 September 2020

KEYWORDS
Plasma focus; time of flight; D-D neutron detection; D-T neutron detection; scattered neutron; fusion chained reactions

1. Introduction

Dese plasma focus (DPF) has always been of interest as intensive pulse neutron source. The hot dense plasma in the pinch column produces thermonuclear and non-thermonuclear (beam-target) fusion neutrons. In the non-thermonuclear process, high-energy ions accelerated away from the anode by electric fields but the high-energy electrons accelerate in the opposite side towards the anode tip. These processes cause fusion neutrons and X-ray emission. Up to date, there are many studies about DPF neutron production and measurements (*1*–*4*). Thermonuclear fusion neutrons are generated in the plasma compression phase and beam-target fusion neutrons are produced in plasma expansion phase (*5*).

The standard time of flight (TOF) spectroscopic method allows the determination of the emitted neutron energy and the number of the particles emitted from the source with high accuracy. Since the neutrons in question are not relativistic, their energy can be directly determined from $E = 1/2mv^2$, where the velocity v is obtained from the distance between the source and the detector, and time interval between HXR as a first peak and neutron as a second peak.

M. S. Rafique et al. (*6*) measured 2.48 ± 0.04 MeV and 3.00 ± 0.09 MeV of energies for D-D neutrons in the radial and the axial directions of DPF, respectively. V. A. Gribkov et al. (*7*) measured the energy of neutrons directly arrived to the scintillator from the DPF chamber equal to 2.7 MeV. F. Castillo et al. (*8*) were performed experiments using the FN-II small plasma focus device, use of the TOF technique. The energies are widely spread form 1.7 MeV

CONTACT A. Raeisdana araeisdana@aeoi.org.ir

up to 3.2 MeV, and in some case, up to 4 MeV. M. Abdollahzadeh et al. (*9*) determined the time dependent neutron energy spectrum in the Filippove type 'Dena' plasma focus, for distances: 5, 10, 18 and 30 m. The measured energy is in the range of 2.5–3 MeV. A. Talaei et al. (*5*) studied on neutron generation mechanism, they presented thermal neutron production in plasma compression phase and beam-target neutron production in plasma expansion phase. Also, Structure of double neutron pulses was obtained by TOF measurements.

2. Experimental setup

The experiments are carried out using the IR-MPF-100 DPF with the deuterium gas at V = 13 kV (E = 12.2 kJ) and p = 1–1.5 mbar. Schematic of the IR-MPF-100 DPF is seen in Figure 1. Fast time-response measurements of neutron emission rate were carried out using plastic scintillator-photomultiplier (PS-PM) detector. NE-102 plastic scintillator coupled with PMT. The NE-102 crystal characterizations were listed in Table 1. To operate the PMT, a high voltage up to 2.3 kV is applied across the cathode and anode with proper distribution of voltages. The PS-PM detector has been located 2.5 m away from the focus region at the angle of 90° with respect to device axis (see Figure 1). All signals have been recorded by Tektronix TDS2024C (200 MHz, 2 GS/s) oscilloscope and time resolution is equal to 1 ns.

Operating Voltage Range (V)	2000 - 2300
Maximum Voltage (V)	2500

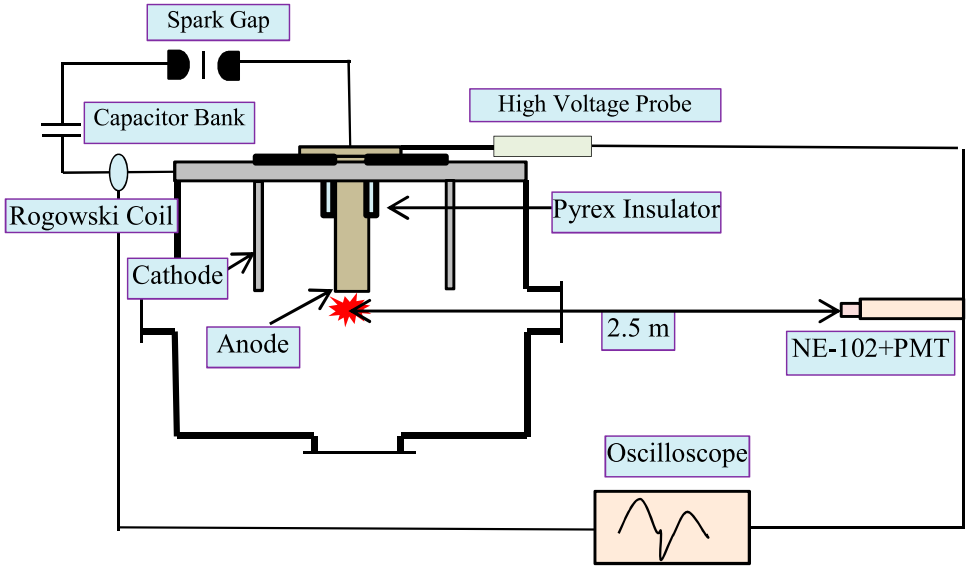

Figure 1. Schematic of the IR-MPF-100 DPF, the PS-PM detector has been located 2.5 m away from the focus region.

Table 1. The plastic scintillator characterizations.

Crystal type	NE-102
Crystal size	4.9 cm × 5.7 cm
Density (g/cm^3)	1.032
Light output Anthracene %	65
Wavelenght of maximum emission (nm)	423
Decay constant (ns)	2.4
Reflective index	1.58
Threshold voltage (V)	1900
Operating voltage range (V)	2000–2300
Maximum voltage (V)	2500

3. Results and discussion

(a) D-D Neutrons

The neutron energy was measured by the PS-PM detector located at 2.5 m away from the focus region at the angle of 90° with respect to device axis. It is worth to mention that the shorter line of sight will provide higher flux incident on the detector and at the same time acceptable sensitivity to the higher energy neutrons. By calculating the time interval between the neutron signal and HXR signal, the velocity and consequently the energy of neutrons are calculated. D-D neutrons were detected with clear and high signal to noise ratio in these experiments. Figure 2 shows the recorded signals for neutron and HXR. Neutron TOF has been measured from the time differences between HXR peak time as a first peak and neutron peak time as a second peak. Also, X-ray traverses the 2.5 m distance between source and detector in 8 ns. So the neutron TOF is equal to 120 ns + 8 ns = 128 ns. The energy of neutrons can be calculated by 128 ns of time and

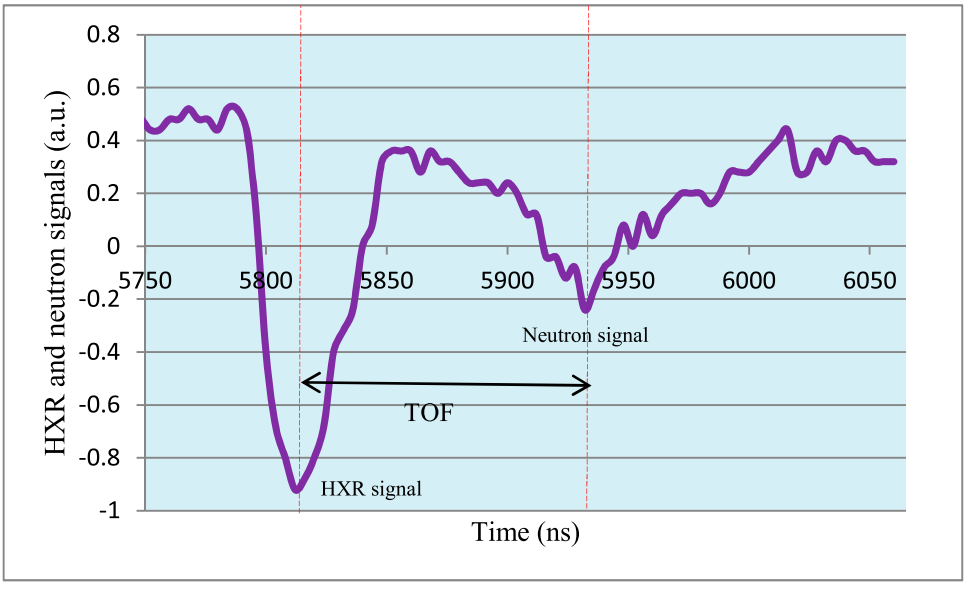

Figure 2. Detecting D-D neutrons using the PS-PM detector housed 2.5 m away from the focus region.

Table 2. FWHM and intensity for neutron beam and HXR beam (Exp.1).

	FWHM (ns)	Beam intensity (a.u.)
HXR	38	52
D-D neutron	57	44

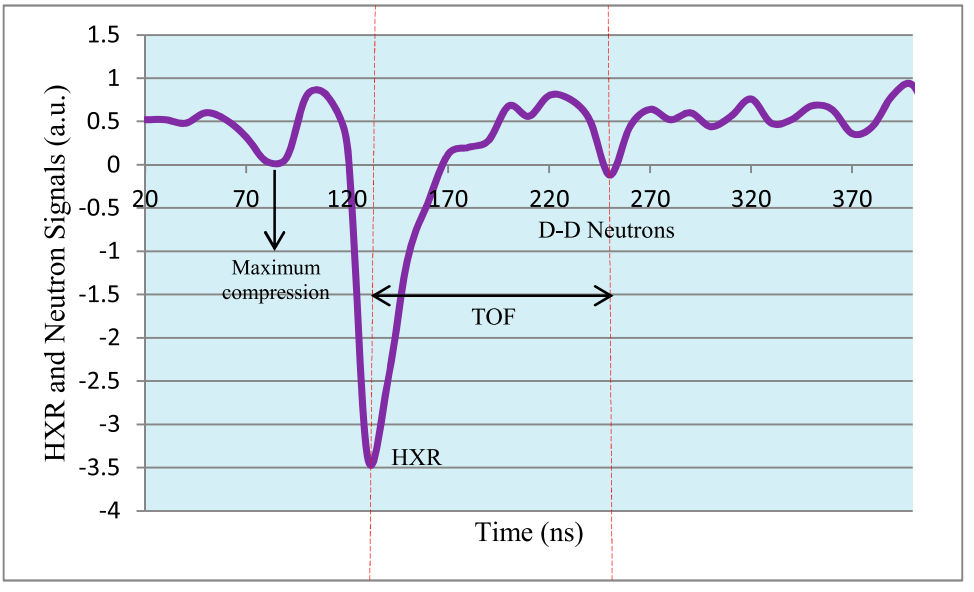

Figure 3. Signals are maximum compression (pinch), HXR and D-D neutrons respectively.

2.5 m of distance. Calculation indicates $1.9966 \sim 2 \pm 0.03$ MeV kinetic energy for neutrons:

$$E = \frac{1}{2}mv^2 = \frac{1}{2}(1.67 \times 10^{-27}) \times \left(\frac{2.5}{128 \times 10^{-9}}\right)^2 = 2.0\,\text{MeV}$$

In Figure 2, the measurement of FWHM for neutron signal and HXR signal results 57 and 38 ns, respectively, which the neutron pulse is clearly wider. For recorded signals by PS-PM detector, area under the curve indicates the beam intensity. In Figure 2, the measurement of neutron intensity and HXR intensity illustrate 52 and 51 a.u. respectively (Table 2).

In experiment 2 (Figure 3), the first signal is the HXR signal with the large amplitude and the second signal is the neutron signal with smaller amplitude. Similar to the previous measurement, TOF is equal to $120 + 8 = 128$ ns and $E_n = 2.0 \pm 0.03$ MeV. Before the HXR signal, a small peak is seen. Probably, it can be related to pinch formation (maximum compression) and its radiations such as soft X-ray (SXR) emission.

(b) D-T Neutrons

D-D fusion reactions are done in two ways $^3\text{He} + \text{n}$ and $\text{T} + \text{p}$. The Produced tritium can be reacted with deuterium and generates 14.1 MeV neutrons. We carried out consecutive deuterium shots (5 shots without chamber vacuuming) until T atoms increase enough so D-T reactions can be detectable. Using this method, we generated 14.1 MeV neutrons without

the tritium injection. In this process, fusion chained reactions are performed. The following equations display fusion chained reactions:

$$D + D \rightarrow {}^{3}He + n\ (2.45\ MeV)$$
$$D + D \rightarrow T + p$$
$$D + T \rightarrow {}^{4}He + n\ (14.1\ MeV)$$

Increasing tritium atoms can lead to significant amount of D-T reactions. We were able to detect D-T neutrons in a few shots (see Figure 4). In Figure 4, regarding to velocity of beams, the observed signals are HXR, D-T neutrons, direct D-D neutrons and scattered D-D neutrons respectively. Time processing displays the interval between the second peak and the first peak is equal to 44 ns so results TOF $= 44 + 8 = 52$ ns and neutron energy equal to 12.09 ± 0.46 MeV which is close to the energy of D-T neutrons. The energy of D-T neutrons and direct D-D neutrons are calculated as:

$$\Delta t = 44\ \text{ns} + 8\ \text{ns} \rightarrow E_{D-T} = 12.09\ \text{MeV}$$
$$\Delta t = 112\ \text{ns} + 8\ \text{ns} \rightarrow E_{D-D\ direct} = 2.27\ \text{MeV}$$

That X-ray TOF (8 ns) has been added to time interval between HXR peak and neutron peak. In addition, FWHM and the area under the curve were computed for each pulse in Figure 4 and listed in Table 3. If the intensity value for the neutron signal (the area under the neutron signal) is calibrated using the known neutron counters such as BF_3, ^3He or Geiger–Mueller activation counter then it would represent the total yield of neutrons.

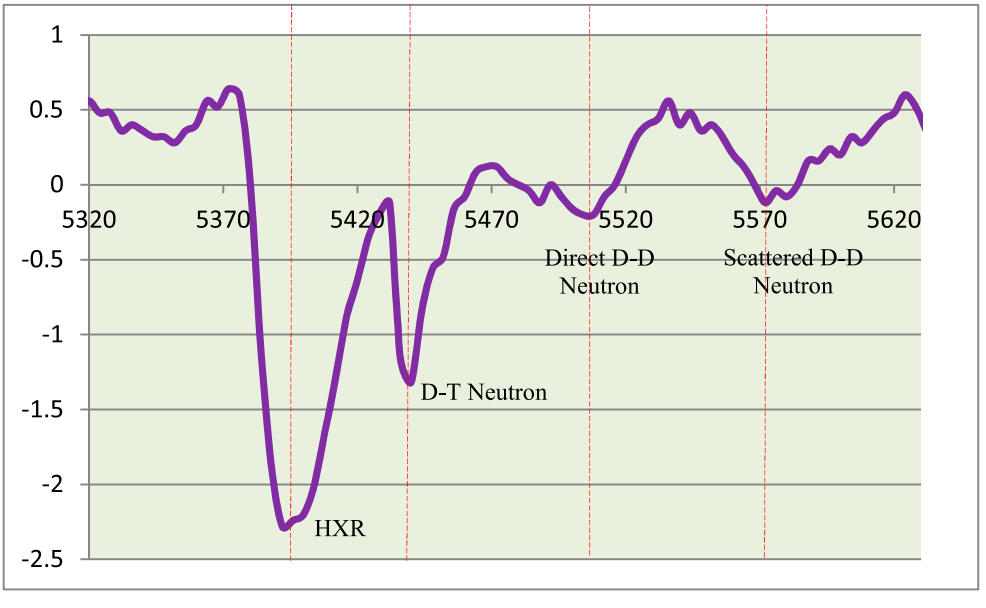

Figure 4. The emitted D-D and D-T neutron signals.

Table 3. FWHM and beam intensity for neutron and HXR (Exp.3).

	FWHM (ns)	Beam intensity (a.u.)
HXR	33	93
D-T neutron	20	37
Direct D-D neutron	48	29
Scattered D-D neutron	33	23

In this experiment, the HXR intensity is more than the D-T and D-D neutron flux. Moreover, D-T neutron pulse is sharper than D-D neutron pulse. In the similar work, D-T neutrons were detected by B. L. Freeman et al. (*1*) in the deuterium shots for TAMU dense plasma focus device and reported the 14.1 MeV daughter neutron pulse.

(c) Scattered Neutrons

In many other experimental shots, two, three or more signals were detected for D-D neutrons that related to the direct neutrons and the scattered neutrons by the surrounding environment (*10*–*14*). Neutrons can be scattered by the chamber, the polyethylene shield and the steel table under the PF. Regarding to the location of the detector (Figure 5), the scattered neutrons from the chamber can reach to the detector.

Neutrons are scattered from all parts of the chamber in all solid angles and reach to the detector but the number of neutrons with the large scattering angles are very low and more neutrons are scattered with the small angles so paths to the detector are approximately equal.

In Exp. 4 (Figure 6), two D-D neutron signals were detected. Time processing results the energy of the direct D-D neutron equal to 2.80 ± 0.05 MeV.

For computing of the energy of scattered neutrons, the path is divided into two parts: AB′ and B′C (see Figure 5). The incident neutrons have the energy of 2.8 MeV in the AB′ path, so:

$$E_{in} = 2.8\ \text{MeV}, \quad AB' = 0.2\ \text{m} \rightarrow t_{AB'} = 8.6\ \text{ns} \rightarrow t_{B'C} = 164 - 8.6 = 155.4\ \text{ns}$$

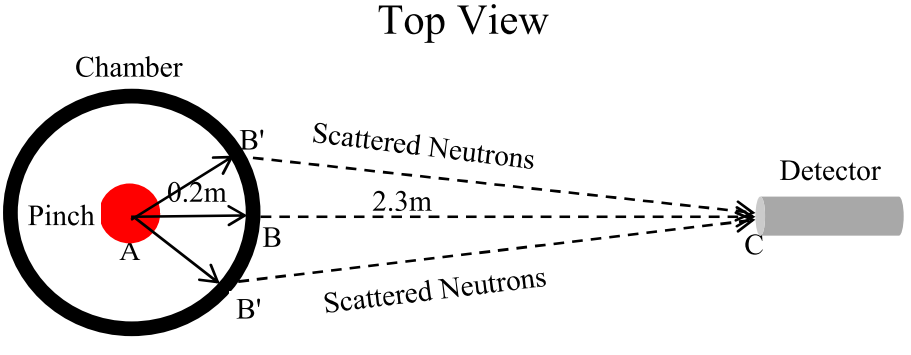

Figure 5. The top view of pinch, chamber and detector, scattered neutrons by chamber are detected in PS-PM detector.

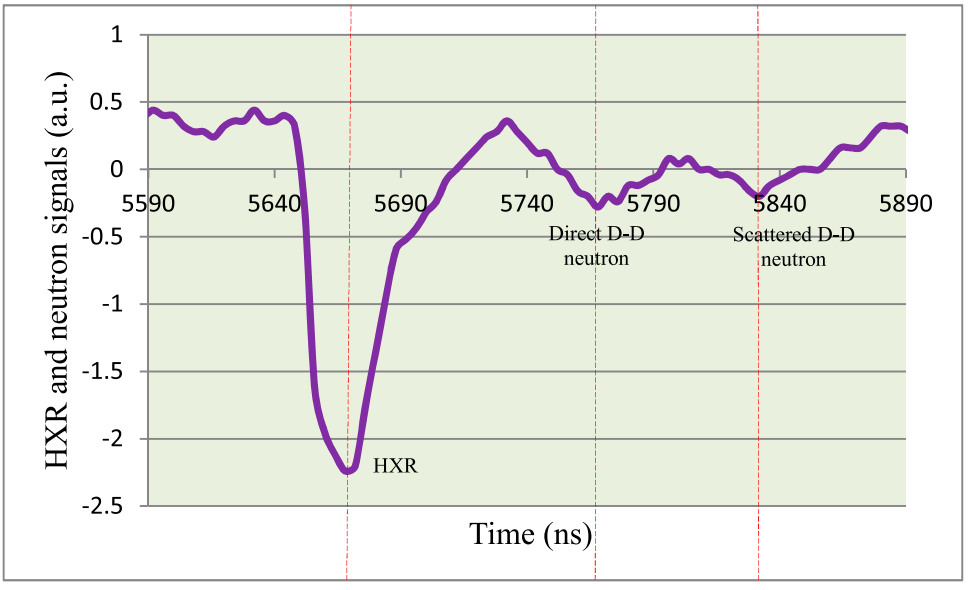

Figure 6. Consecutive neutron signals, including direct neutrons and scattered neutrons.

Table 4. Emission duration and intensity for neutron beam and HXR beam (Exp.4).

	FWHM (ns)	Beam intensity (a.u.)
HXR	31	96
Direct D-D neutron	52	31
Scattered D-D neutron	53	29

That E_{in} is the energy of the incident neutrons. For small angle of scattering can be write $B'C \sim BC = 2.3$ m and the error is very small. By having the time and the distance, the energy of scattered neutrons E_{sc} can be calculated for the $B'C$ path:

$$B'C \sim 2.3\ \text{m}, \quad t_{B'C} = 155.4\ \text{ns} \rightarrow E_{sc} = 1.14\ \text{MeV}$$

The similar computations for Figure 4 results $E_{sc} = 0.86$ MeV.

For this Figure, FWHM and the beam intensity were also measured (Table 4). Similar to the previous experiments, FWHM of neutron signals are longer than the FWHM of HXR signal while HXR intensity is more than the neutron intensity.

4. Conclusion

In this work, D-T neutrons were generated by consecutive deuterium shots and detected by PS-PM detector. Repeating deuterium shots increase the rate of tritium atoms and it is enabled the D-T fusion reactions. The element of novelty of this work is the generation of D-T neutrons by deuterium shots. 2.5 m distance between detector and focus region was caused the separation between HXR signal and neutron signals. Shorter selected line of sight causes higher neutron flux incident, good visibility and acceptable sensitivity for HXR and neutron signals. Besides that, D-D neutrons and scattered D-D neutrons were

detected and their energies were measured. The measurement of neutron energy results (2–2.8) ± 0.05 MeV for D-D reactions and 12.09 ± 0.46 MeV for D-T reactions when detector is at the angle of 90^0 with respect to device axis. Multiple neutron signals are detected due to neutron scattering from the surrounding environment.

Duration of neutron emission can be derived using FWHM of neutron pulse and FWHM of HXR pulse. For HXR pulse, all photons travel with light velocity c, therefore the pulse broadening is due to the duration of the HXR emission. About neutron pulse, neutrons are not monoenergetic and pulse broadening occurs due to both duration of the neutron emission and non-monoenergetic neutrons. HXR and neutron are emitted in plasma expansion phase and we can consider their duration of emission is equal. So, we can result:

$$\text{Broadening of neutron pulse due to non-monoenergetic neutrons} = \text{FWHM}_n - \text{FWHM}_x$$

That FWHM_n is the FWHM of neutron pulse and FWHM_x is the FWHM of HXR pulse.

According to above equation, the range of neutrons energy can be obtained. For example in Figure 2, broadening of neutron pulse = 57–38 = 19 ns which results the neutron energy in the range of 1.51 MeV to 2.75 MeV. For Figure 4, the broadening of neutron pulse = 48–33 = 15 ns which results the neutron energy in range of 1.79–2.97 MeV. For Figure 5, neutron pulse broadening is equal to 21 ns and the range of neutrons energy is equal to 1.96–4.32 MeV.

Scattered neutrons from chamber were detected and studied. TOF method results 1.14 and 0.86 MeV of energies for scattered neutrons.

Disclosure statement

No potential conflict of interest was reported by the author(s).

References

(1) Freeman, B.L.; Boydston, J.C.; Ferguson, J.M.; Lindeburg, B.; Luginbill, A.D.; Rock, J.C.; Tutt, T.E.; Hagen, E.C.; Ziegler, L. Neutron Emission Characteristics of a High-Current Plasma Focus: Initial Studies. In *14th International Conference on High-Power Particle Beams (BEAMS)*Albuquerque, NM, 2002.

(2) Damideh, V.; Saw, S.H.; Sadighzadeh, A.; Ali, J.; Rawat, R.S.; Lee, P.; Lee, S. PMT-scintillator System Set Up for D-D Neutron TOF Measurements in INTI Plasma Focus Device. In *AIP Conference Proceedings, March 2017*, Langkawi, Malaysia, 2017; Vol. 1824, pp 281–288. DOI: 10.1063/1.4978846.

(3) Borthakur, T.K.; Shyam, A. Analysis of Axial Neutron Emission Pulse from a Plasma Focus Device. *Indian Journal of Pure & Applied Physics* **2010,** *48*, 100–103.

(4) Lemeshko, B.D.; Dulatov, A.K.; Mikhailov, Yu.V.; Prokuratov, I.A.; Selifanov, A.N.; Fatiev, T.S.; Andreev, V.G. Lifetime and Shelf Life of Sealed Tritium-Filled Plasma Focus Chambers with gas Generator. *Matter and Radiation at Extremes* **2017,** *2*, 303–308.

(5) Talaei, A.; Sadat Kiai, S.M.; Adlparvar, S. Pinched Plasma Study in a Filippov-Type Plasma Focus 'Dena'. *IEEE Trans. Plasma Sci.* **2008,** *36* (3), 794 –801 .

(6) Rafique, M.S.; Serban, A.; Lee, P.; Lee, S. Neutron and Soft X-ray Emission from Plasma Focus. In *26th EPS Conf. on Contr. Fusion and Plasma Physics*, EPS Conference : Maastricht, Netherlands, 1999; Vol. 23, pp 1249–1252.

(7) Gribkov, V.A.; Banaszak, A.; Bienkowska, B.; Dubrovsky, A.V.; Ivanova-Stanik, I.; Jakubowski, L.; Karpinski, L.; Miklaszewski, R.A.; Paduch, M.; Sadowski, M.J. Plasma Dynamics in the PF-1000 Device under Full-Scale Energy Storage: II. Fast Electron and Ion Characteristics versus Neutron Emission Parameters and Gun Optimization Perspectives. *Journal of Physics D-Applied Physics* **2007,** *40* (12), 3592–3607.

(8) Castillo, F.; Gamboa, I.; Herrera, J.J.E.; Rangel, J. Neutron Emission Characterisation at the FN-II Dense Plasma Focus. *J. Phys: Conf. Ser.* **2014**. DOI: 10.1088/1742-6596/511/1/012021.
(9) Abdollahzadeh, M.; Sadat kiai, S.M.; Babazadeh, A.R. Measurement of the Time Dependent Neutron Energy Spectrum in the 'DENA' Plasma Focus Device. *Plasma Phys. Controlled Fusion*. **2008,** *50* (10), 218–222.
(10) Schmidt, D.; Zuying, Z.; Xichao, R.; Hongqing, T.; Bujia, Q.; Haihong, X.; Jianrong, D. Application of Non-Monoenergetic Sources in Fast Neutron Scattering Measurements. *Nuclear Instruments and Methods in Physics Research A*. **2005,** *545*, 658–682.
(11) Gribkov, V.A. A Dense Plasma Focus-Based Neutron Source for a Single-Shot Detection of Illicit Materials and Explosives by a Nanosecond Neutron Pulse. *Phys. Scr.* **2010,** *81* (3), 035502.
(12) Buffler, A.; Brooks, F.D.; Aschman, D.G. Doctoral Thesis, Fast Neutron Scattering Analysis, University of Cape Town, Faculty of Science, Department of Physics, 1998.
(13) Brooks, F.D. Determination of HCNO Concentrations by Fast Neutron Scattering Analysis. *Nuclear Instruments and Methods in Physics Research Section A* **1998,** *410* (2), 319–328.
(14) Tartaglione, A. Detection of Water by Neutron Scattering Using a Small Plasma Focus. *Braz. J. Phys.* **2004,** *34* (4B), 1756–1758.